

# Modeling multiple curved fractures connected through a wellbore using a fluid-coupled XFEM algorithm

Abbas, S.

*Schlumberger, Sugar Land, TX, USA*

Gordeliy, E.

*Schlumberger-Doll Research Center, Cambridge, MA, USA*

Peirce, A.

*University of British Columbia, Vancouver, British Columbia, Canada*

Copyright 2016 ARMA, American Rock Mechanics Association

This paper was prepared for presentation at the 50<sup>th</sup> US Rock Mechanics / Geomechanics Symposium held in Houston, Texas, USA, 26-29 June 2016. This paper was selected for presentation at the symposium by an ARMA Technical Program Committee based on a technical and critical review of the paper by a minimum of two technical reviewers. The material, as presented, does not necessarily reflect any position of ARMA, its officers, or members. Electronic reproduction, distribution, or storage of any part of this paper for commercial purposes without the written consent of ARMA is prohibited. Permission to reproduce in print is restricted to an abstract of not more than 200 words; illustrations may not be copied. The abstract must contain conspicuous acknowledgement of where and by whom the paper was presented.

**ABSTRACT:** A significant challenge in horizontal well stimulation is the ability to simultaneously generate multiple hydraulic fractures (HF) with roughly uniform dimensions within a single stage. When the fractures are relatively close, the outer fractures in a stage exert a strong confining stress on the inner fractures, inhibiting their development and the desired uniform growth of fractures in the stage. There is thus a need to develop computational tools to analyze this mutual interaction between propagating HF to seek designs that can mitigate this inhibition phenomenon which is known as stress shadowing. In this paper, we report the development of an axisymmetric extended finite element method (XFEM) that can model multiple simultaneously propagating HF that are able to curve (forming bowl-shaped fractures) and which is able to autonomously partition the flux of fluid among the HF in the stage. To test the flux partitioning algorithm, we compare the XFEM code to a parallel planar displacement discontinuity (DD) code. To test the HF curving due to mutual interaction, we compare the XFEM to an axisymmetric DD code, which can model two symmetric fractures that can curve due to mutual interaction. Finally, we describe an experiment in which five mutually interacting HF with flux partitioning are allowed to curve, and we compare the results to the case in which the five HF are constrained to develop in distinct parallel planes.

## 1. INTRODUCTION

Horizontal wells frequently have a significant number of nonproducing perforation clusters in a given stage due to variations in the reservoir properties and the phenomenon of stress shadowing, in which the confining stress induced by the outer fractures in a stage serves to inhibit the growth of the inner fractures. It is thus desirable to develop computational tools that can analyze such situations to determine the optimal choice of engineering parameters to mitigate the effect of stress shadowing and reservoir heterogeneity. A complete model of this situation requires a fully coupled 3D simulator that can model curving HF that simultaneously propagate in a heterogeneous solid medium. Thus far, models of this situation have been restricted to homogeneous media involving pseudo-3D approximations that can admit curving cracks (Kresse et al., 2013), 2D-axisymmetric HF that are assumed to grow in parallel planes (Lecampion and Desroches, 2015) or arbitrarily shaped HF that are assumed to grow in parallel planes (Bunger and Peirce, 2014; Peirce and Bunger, 2015).

A fully coupled XFEM algorithm has recently been developed by the authors (Gordeliy and Peirce, 2013, 2015) for HF propagation, and applications have been restricted to plane strain HF. The work reported in this paper describes the development of an axisymmetric XFEM code that is able to model multiple interacting cracks (which, due to the axisymmetry, will be bowl-shaped) and which is able to autonomously partition the fluid pumped into the horizontal well among the developing fractures in the stage under investigation – a process we refer to as flow diversion. A number of numerical results are presented. The XFEM model developed in this paper is compared to a 3D displacement discontinuity (DD) model ILSA (Bunger and Peirce, 2014; Peirce and Bunger, 2015) that is able to model multiple planar HFs that are assumed to be propagating in parallel planes with flow diversion. To test the validity of the algorithm for modeling curving of the fractures due to mutual interaction, the XFEM is compared to an axisymmetric DD model OribiC (Gordeliy and Detournay, 2011), which, in turn, has been validated against laboratory experiments for bowl-shaped fractures near a free surface (Bunger et al., 2013). Finally, five

mutually interacting HF with flux diversion are allowed to curve, and the results are compared with the situation in which the five fractures are constrained to develop in distinct parallel planes.

The remainder of the paper is organized as follows: in section 2, we describe the model, including the governing equations for fluid flow and elasticity; in section 3, we briefly describe the XFEM model and provide the numerical results; in section 4, we make some concluding remarks.

## 2. MODEL DESCRIPTION

We consider a horizontal well drilled in the direction of the minimum horizontal stress  $\sigma_h$ . We assume that the elastic parameters (Young's modulus  $E$  and Poisson's ratio  $\nu$ ) and the in-situ stress components (minimum horizontal stress  $\sigma_h$  and the maximum horizontal stress  $\sigma_H$ , which is assumed to be equal to the vertical stress component) are constant in the radial direction orthogonal to the wellbore. This assumption allows us to restrict ourselves to fractures that grow in an axisymmetric fashion away from the horizontal wellbore. The fracture growth is assumed to be driven by a Newtonian fluid of dynamic viscosity  $\mu$  from an injection point located at the center of the axisymmetric fracture. This point source represents a perforation cluster in a multistage hydraulic fracturing treatment. The fluid is pumped in the wellbore at a constant volumetric injection rate  $Q_0$ . In multistage hydraulic fracturing, multiple fractures are propagated simultaneously in each stage. These fractures are assumed to affect each other elastically in the rock-mass and hydraulically within the wellbore. We model both of these interactions. The elastic interaction is modeled by the domain-based extended finite element method (XFEM) and the hydraulic interaction is modeled by a fluid flux-splitting algorithm. The fractures are allowed to curve due to their mutual elastic interaction. The curving of an axisymmetric fracture results in a bowl-shaped fracture.

### 2.1. Elasticity

The balance of forces is given by the following equilibrium equation:

$$\nabla \cdot \boldsymbol{\sigma} + \mathbf{f} = \mathbf{0} \quad (1)$$

in which  $\mathbf{f}$  is the body force and  $\boldsymbol{\sigma}$  represents the stress field in the domain, which is related to the strain tensor  $\boldsymbol{\varepsilon}(\mathbf{u})$  through the following constitutive relation

$$\boldsymbol{\sigma} = \mathcal{C} : \boldsymbol{\varepsilon}(\mathbf{u}) \quad (2)$$

The strain tensor  $\boldsymbol{\varepsilon}(\mathbf{u})$  is related to the displacement field  $\mathbf{u}$  by the following relation:

$$\boldsymbol{\varepsilon}(\mathbf{u}) = \frac{1}{2} (\nabla \mathbf{u} + (\nabla \mathbf{u})^T) \quad (3)$$

The displacement  $\mathbf{u}$  and the stress field  $\boldsymbol{\sigma}$  are the primary elastic unknowns defined in Cartesian coordinates by components  $u_i$  and  $\sigma_{ij}$ . In Eqs. (1) and (2), tensile stresses are assumed to be positive; however, we switch to a positive compressive stress convention in the following for convenience. The fracture opening is represented by the normal displacement jump across the fracture faces:

$$[[\mathbf{u}]] \cdot \mathbf{n} = (\mathbf{u}^+ - \mathbf{u}^-) \cdot \mathbf{n} = w \quad (4)$$

### 2.2. Fluid Flow

We neglect the fluid compressibility with respect to the fracture compliance. The mass balance is then reduced only to the volume balance given by the continuity equation

$$\frac{\partial w}{\partial t} + \frac{1}{r} \frac{\partial}{\partial s} (rq) = 0 \quad (5)$$

where  $r$  is the radial coordinate along the radius of the axisymmetric fractures, and  $s$  is the arc-length coordinate along the one-dimensional representation of an axisymmetric fracture in the  $(r, z)$  axes. The fluid flux  $q$  inside the fracture follows Poiseuille's law, under the hypothesis of low Reynold's number flow that is assumed in lubrication theory. Poiseuille's law relates the variation of the fracture width  $w$  and the pressure gradient  $\frac{\partial p}{\partial s}$  to the fluid flux  $q$  within the fracture:

$$q = -\frac{w^3}{\mu'} \frac{\partial p}{\partial s}, \quad (6)$$

in which  $\mu' = 12\mu$  where  $\mu$  is the dynamic fluid viscosity. A fluid lag may develop between the fluid front and the fracture front during the hydraulic fracturing process. The timescale associated with the development of such a lag is given by:  $t = \frac{E^2 \mu'}{(1-\nu^2)^2 \sigma_0^3}$  (Bunger, 2005; Gordeliy and Detournay, 2011), where  $\sigma_0$  is the confining stress. This timescale is inversely proportional to  $\sigma_0^3$ . Accordingly, we can ignore the fluid lag due to the high confining stress normally encountered in deep formations. The appropriate boundary conditions at the fracture tip (Detournay and Peirce, 2014) are that the fluid flux and the fracture width are thus assumed to vanish:

$$w(r) = 0, \quad q(r) = 0 \quad (7)$$

where  $r = R_i$  and  $R_i$  is the radius of fracture  $i$ . At the fracture inlet, pressure continuity is ensured by considering the fluid pressure  $p_f$  at the fracture inlet to equal the wellbore pressure  $p_{wb}$ , i.e.,

$$p_f(r = 0) = p_{wb} \quad (8)$$

We ignore the pressure drop at the inlet due to perforation friction.

### 2.3. Multiple Fracture Initiation and Propagation

During the initial fracture propagation, the energy dissipation in breaking the rock is less than the energy dissipated in pushing the viscous fluid through the fracture. Fracture propagation under this condition is called viscosity-dominated fracture propagation. We take the analytical solution for the viscosity-dominated fracture propagation ( $M$  vertex solution) for the penny-shaped fracture in an infinite medium (Savitski and Detournay, 1999) as the initial solution. In the case of multiple axisymmetric fracture propagation, the fluid flux into each fracture, which is typically different for each fracture in a stage, is found by an iterative procedure such that the pressure at each fracture inlet is equal to the wellbore pressure and the sum of all the fluxes going into each fracture  $q_i$  is equal to the total flux  $Q_0$  pumped into the wellbore, i.e.,

$$\sum q_i = Q_0 \quad (9)$$

Finally, the initial pressure and width distribution inside each fracture is assumed to satisfy the corresponding  $M$  vertex solution.

## 3. NUMERICAL SCHEME

We use the mixed hybrid XFEM scheme developed by (Gordeliy and Peirce, 2013; Abbas et al., 2014) to solve for the fluid flow and elastic deformations in a coupled manner. The elastic effects of the fracture are given by the XFEM formulation (Fries and Belytschko, 2010) that represents the discontinuous and singular fields in the finite element mesh. In the current application, we consider the fluid front to coincide with the fracture front, which results in a singular pressure field near the fracture tip. This creates considerable challenges for computing the fracture opening using only the fluid pressure (the so-called Neumann to Dirichlet map). For this purpose, the fracture is divided into two regions. The first is the larger region away from the crack tip, in which we solve for the fracture width assuming a prescribed fluid pressure boundary condition. The second is the tip region, in which the fracture width asymptote acts as a boundary condition on the fracture width and is prescribed according to the applicable tip asymptote. The discretized weak form for the XFEM is described in detail for the plane-strain case by Gordeliy and Peirce (2015). In the current application, additional terms that represent the hoop stress and strain are added to the weak form. Integration of the weak form involves multiplying the integrands by a  $2\pi r$  factor to account for the axisymmetric formulation.

The fluid flow Eqs.(5) and (6) are discretized using the finite volume scheme described in Gordeliy and Peirce

(2013). The XFEM provides the fracture width in terms of a given fluid pressure. This solution is then used to eliminate the fracture width from the discretized fluid flow equations. These equations are then solved iteratively using Newton's method until the pressure converges to an equilibrating fluid pressure in the channel region. This pressure is then used in the XFEM scheme to provide the corresponding fracture widths. The direction of fracture propagation is found through a maximum tensile stress condition (Erdogan and Sih, 1963). The curved fracture geometry is represented by the hybrid explicit-implicit crack description of Fries and Baydoun (2012).

During the fracture propagation, the fracture front is located using the implicit level set algorithm (ILSA) (Peirce and Detournay, 2008) in which the viscous tip asymptote of Desroches, et al. (1994) is used to determine the fracture tip position that is consistent with a weak-form tip width asymptote and a pressure field that satisfies local volume balance.

In the following, we validate the fluid flux diversion algorithm with an existing ILSA simulator that can treat multiple simultaneously evolving and interacting hydraulic fractures that are assumed to be propagating in distinct parallel planes. We also validate the fracture curving component of the XFEM algorithm using the DD-based algorithm OriBiC, which was designed to model radially symmetric bowl-shaped fractures. Finally, we study the combined effect of flow diversion and fracture curving on the propagation of five equally spaced fractures.

### 3.1. Validation of Flow Diversion

First we validate our algorithm for flow diversion. We use a test case from Bungler and Peirce (2014) involving the simultaneous propagation of five parallel radial planar fractures with automatic flow rate diversion. The following parameters for the simulation were used:  $E = 9.5$  GPa,  $\nu = 0.2$ ,  $\mu = 1$  Pa.s,  $Q_0 = 0.1$  m<sup>3</sup>/s,  $H = 30$  m and  $\sigma_{zz}^0 = 70$  MPa. Here  $H$  represents the uniform distance between the fractures, and  $\sigma_{zz}^0$  is the confining stress on each fracture. The fractures affect each other through stress shadowing, which is why the outer fractures outgrow the inner fractures. This is visible in the Figure 1. The solid lines represent the results of Bungler and Peirce (2014), and the dashed lines represent the XFEM results. It can be seen that the fracture length growth and the stress shadow effect are accurately modeled by the XFEM.

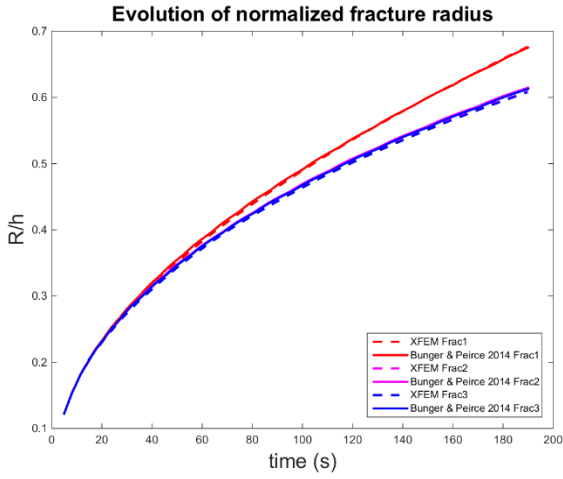


Figure 1: Evolution of normalized fracture radius vs. time for the outer fracture 1 and the inner fractures 2 and 3. We only show the first two fractures and the middle fracture due to the symmetry of the problem.

Figure 2 shows the evolution of the fracture width at the inlet from Bungler and Peirce (2014) compared with the XFEM results. The results from the two algorithms have some initial discrepancy due to slightly different initial conditions, but they rapidly converge and show close agreement. Finally, in Figure 3, we see that the flow rates entering each fracture show close agreement between the two algorithms. Although there is some difference between the results from both methods, the relative difference is less than 5%. This verifies the validity of the flow-division algorithm used for the XFEM multiple fracture simulation.

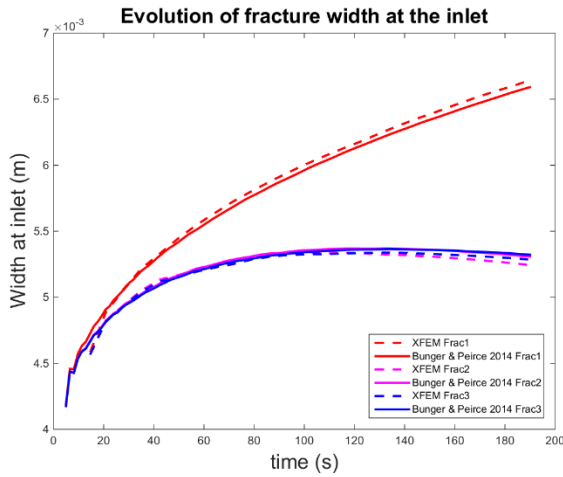


Figure 2: Evolution of fracture width for the outer fracture 1 and the inner fractures 2 and 3.

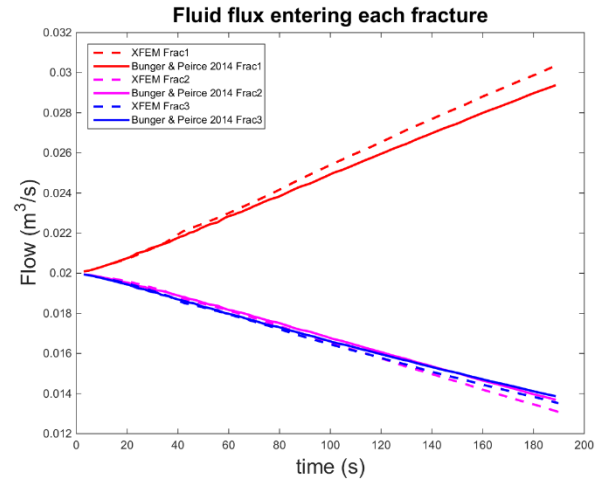


Figure 3: Fluid flux entering each fracture in time.

### 3.2. Validation of the Fracture Curving Algorithm

In this section, we consider two interacting fractures to validate the implementation of the nonplanar fracture propagation in the coupled XFEM model. We compare the results of the present model with the results of an algorithm OriBiC (Bunger et al., 2013) based on the axisymmetric displacement discontinuity method (Gordeliy and Detournay, 2011). The implementation of OriBiC used in (Bunger et al., 2013) included a single fracture with fluid lag, and the fracture propagation was modeled according to a mixed-mode propagation criterion based on the values of the mode *I* and *II* stress intensity factors and the fracture toughness  $K_{IC}$  - consistent with the maximum tensile stress criterion of (Erdogan and Sih, 1963). To model interacting nonplanar fractures propagating in the viscosity-dominated regime in the present paper, we modified OriBiC to include two symmetric bowl-shaped fractures completely filled with the fluid and with an enforced fracture propagation condition corresponding to the viscous tip asymptote of (Desroches et al. 1994). The direction of fracture propagation was determined according to the maximum tensile stress criterion of (Erdogan and Sih, 1963).

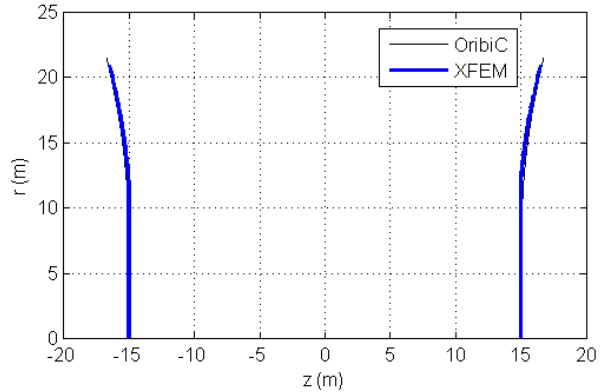


Figure 4: Trajectories of two interacting bowl-shaped fractures. The fractures are shown in the cylindrical coordinates  $(r, z)$ , where the  $z$ -axis is the axis of symmetry.

The XFEM and OriBiC models were used to simulate the propagation of two bowl-shaped fractures initiated a distance 30 m apart (Figure 4). The two fractures were initiated as flat, parallel, and radial with radii 5.4 m and set to the  $M$ -vertex solution (Savitski and Detournay, 1999). Because the fractures were assumed to propagate in the viscosity-dominated regime, the fracture toughness was not involved in the simulations. The far-field axisymmetric confining stresses in the cylindrical coordinate axes  $(r, z)$  were set to  $\sigma_{rr} = \sigma_{zz} = 70$  MPa, and the properties of the rock were Young's modulus  $E = 9.5$  GPa and Poisson's ratio  $\nu = 0.2$ . The viscosity of the injected fluid and the total injection rate were set, correspondingly, to  $\mu = 1$  Pa.s and  $Q_0 = 0.1$  m<sup>3</sup>/s. In OriBiC, we used axisymmetric displacement discontinuity elements of uniform length 0.075 m [in  $(r, z)$  axes]; the fracture was extended by one element at each step, and the corresponding time step was determined from the propagation condition. In the XFEM, the size of the finite elements in the radial direction was set to 0.3 m, and a uniform time step of 0.7355 s was used.

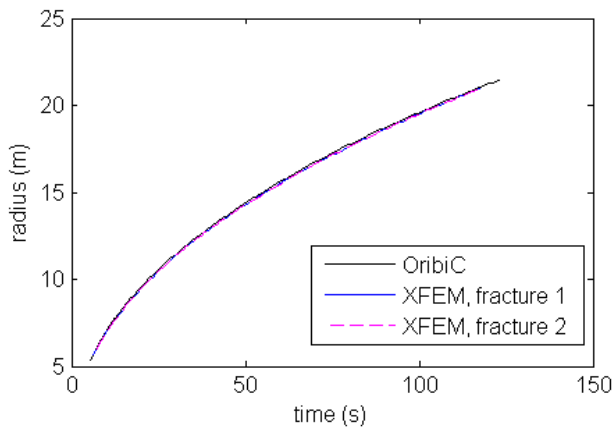


Figure 5: Evolution of fracture radii for two interacting bowl-shaped fractures.

Figure 4 shows the trajectories of the two interacting bowl-shaped fractures obtained from the two models. Figure 5–Figure 7 show the evolution of the fracture radius, fracture width at the wellbore inlet, and the fluid pressure at the wellbore inlet for each fracture. The inlet fluid pressure was obtained by extrapolation of nodal pressures to the wellbore wall. Figure 8 shows the profile of the fluid pressure in each of the fractures at time  $t = 99$  s. In these figures, fracture 1 and fracture 2 refer to the fracture initiated at  $z = 15$  m and at  $z = -15$  m,

respectively.

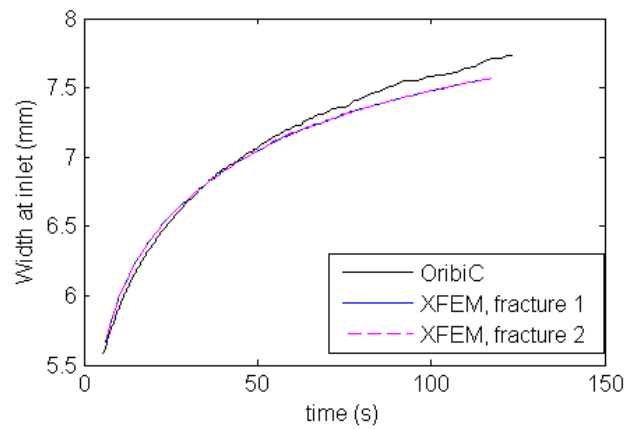


Figure 6: Inlet crack width for two interacting bowl-shaped fractures.

The results of the two models agree well. A small discrepancy in the inlet crack width (Figure 6) and in the wellbore pressure (the inlet fluid pressure in Figure 7) can be due to the different levels of discretization of the fractures in each model. In particular, in the XFEM, the fracture surface near the wellbore was discretized into elements of length 0.3 m (consistent with the finite element size in the radial direction), which is four times larger than the element size of 0.075 m used in OriBiC. Despite the small discrepancy in the wellbore pressures in Figure 7, in Figure 8 the XFEM fluid pressures within the fractures are close to the OriBiC results.

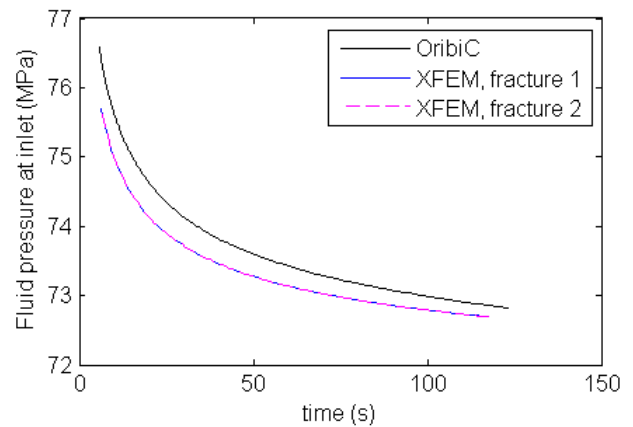


Figure 7: Inlet fluid pressure for two interacting bowl-shaped fractures.

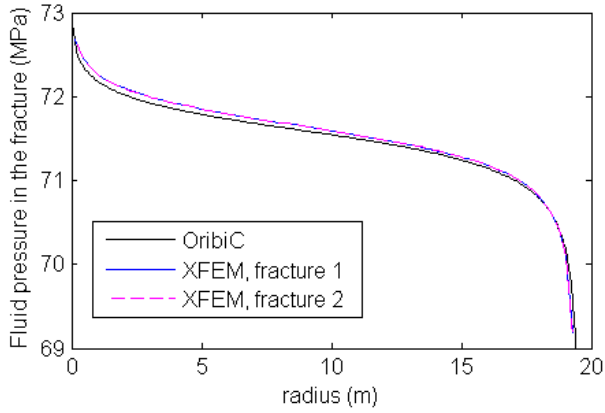


Figure 8: Profile of fluid pressure in each fracture at time  $t = 99$  s.

### 3.3. Effect of Curving and Flow Diversion

Finally, we investigate the effect of fracture curving on fracturing parameters. We want to quantify the effect of fracture curving on the critical hydraulic fracturing variables, namely, the fracture opening at the inlet, the pressure at the fracture inlet, and the fluid flux entering each fracture. Here we present results from two numerical experiments. In each we consider two different cases with the same parameters. The only difference is that in the first case we allow the fractures to curve with automatic flow diversion and in the second case we do not allow the fracture curving. We allow the fractures to grow up to 1.5 times the distance between the fractures and monitor the effect on the fracture characteristics.

In the first experiment, we consider the following parameters: Young's modulus  $E = 9.5$  GPa, Poisson's ratio  $\nu = 0.2$ , dynamic fluid viscosity  $\mu = 1$  Pa.s, total injection rate in the wellbore  $Q_0 = 0.1$  m<sup>3</sup>/s, distance between fractures  $H = 10$  m, minimum horizontal stress acting normal to the initial fracture plane  $\sigma_{zz}^0 = 70$  MPa and the radial stress acting in the initial fracture plane  $\sigma_{rr}^0 = 72$  MPa. The fracture path for all five fractures is shown in Figure 9 for the case of curving fractures. It is shown that the external fractures grow more than the internal fractures. The fractures next to the outer fractures are curved slightly inwards due to the strong stress shadow interaction with the outer fractures.

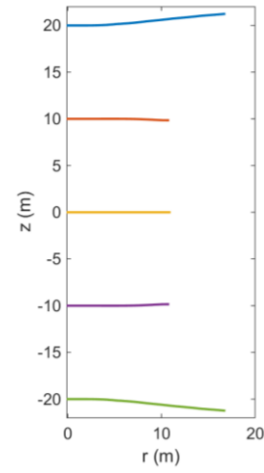


Figure 9: Fracture propagation path for five fractures with curving and flow diversion.

Figure 10–Figure 13 show the effect of fracture curving versus no curving (“flat”) on the fracture length, inlet flow rate, fracture width at the inlet and the inlet pressure. We only show the first two fractures and the middle fracture due to the symmetry of the problem. It can be seen that there is no significant effect of fracture curving on the fracture length. Similarly, there is no significant difference in the inlet flow rate, the fracture width, or the inlet pressure due to fracture curving. This shows that ignoring the fracture curving due to the stress shadow does not cause a significant error in the hydraulic fracturing diagnostics in conditions of this example due to the little curving observed.

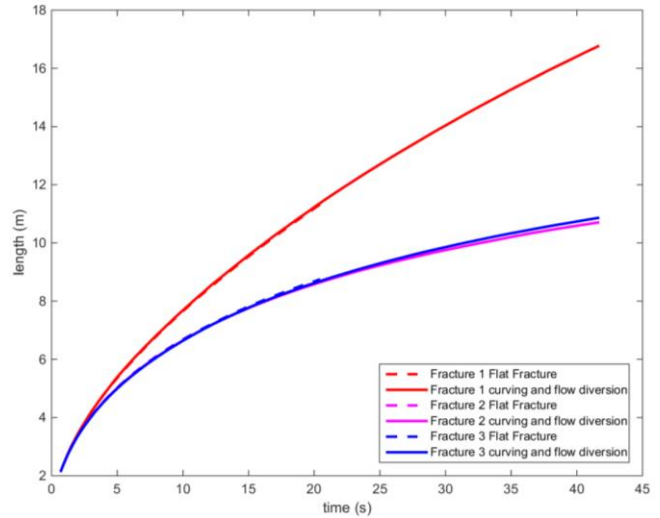


Figure 10: Fracture length vs. time for the flat fractures and the curving fractures.

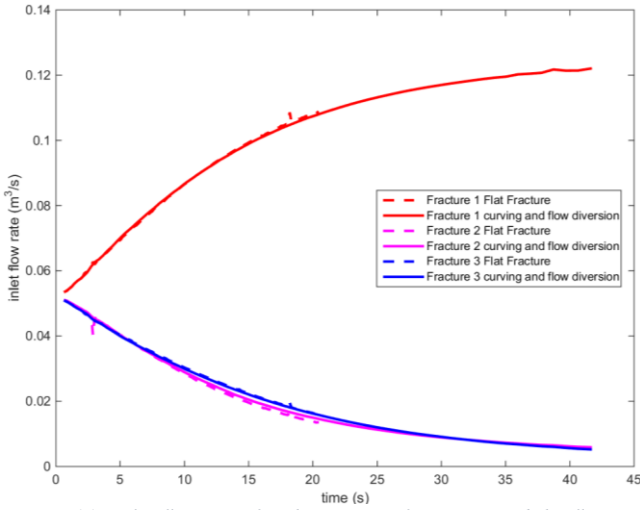


Figure 11: Inlet flow rate for the curving fractures and the flat fractures.

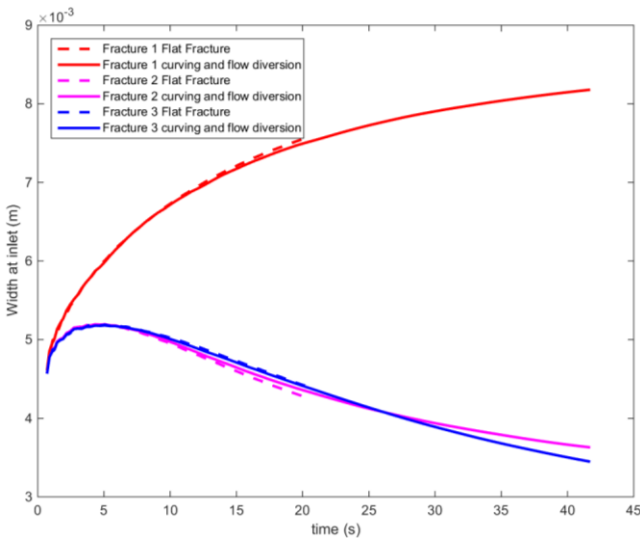


Figure 12: Fracture width at the inlet for curved fractures and the flat fractures.

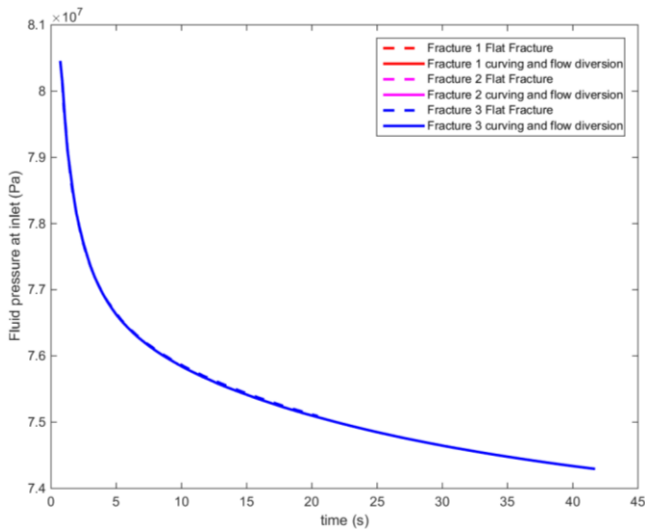


Figure 13: Fluid pressure at the inlet for curved fractures and the flat fractures.

In the second experiment, we use the same parameters as before except for the total injection rate  $Q_0 = 0.05 \text{ m}^3/\text{s}$  and the in situ stress with an isotropic confining stress

condition, i.e.  $\sigma_{zz}^0 = \sigma_{rr}^0 = 70 \text{ MPa}$  (no difference between the radial and the normal horizontal stress acting on the initial fracture plane). The resulting fracture paths in Figure 14 show more pronounced fracture curving in this case. As a result of this there are more pronounced effects on the fracture lengths. As shown in Figure 15, the internal fractures in the case of flat fractures have smaller lengths than the corresponding curving fractures. This results in pronounced effects in the inlet flow rate distribution as well as the pressure and fracture width at the fracture inlet as shown in Figure 16, Figure 17 and Figure 18 respectively. So, taking the fracture curving into account changes the basic hydraulic fracturing diagnostics.

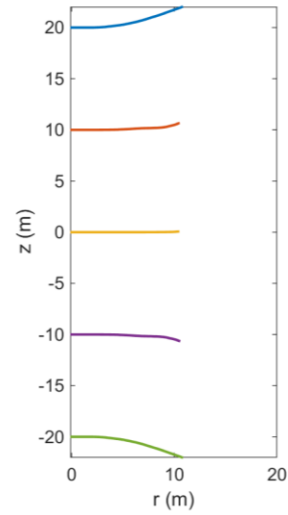


Figure 14: Fracture propagation path for five fractures with curving and flow diversion (isotropic confining stress).

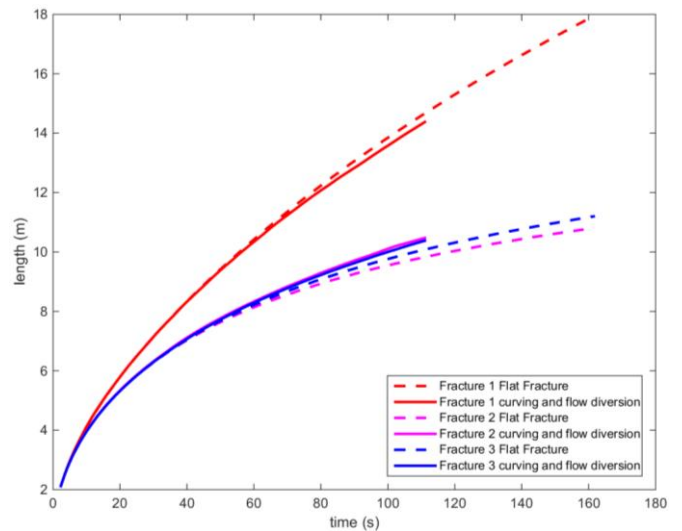


Figure 15: Fracture length vs. time for the flat fractures and the curving fractures (isotropic confining stress).

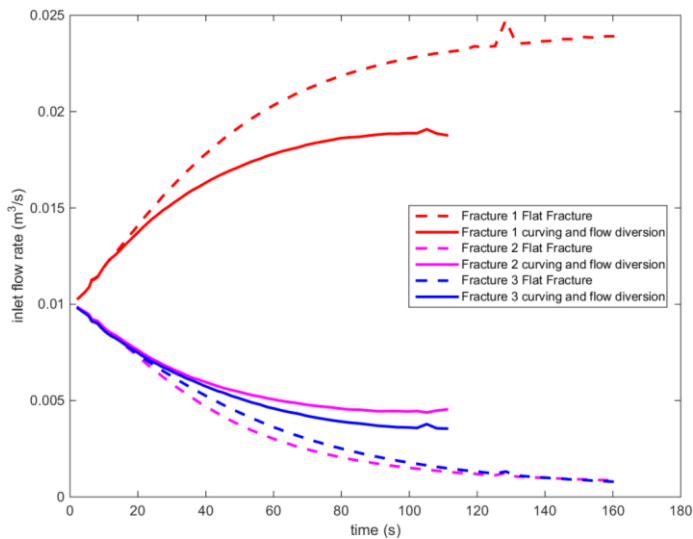


Figure 16: Inlet flow rate for the curving fractures and the flat fractures (isotropic confining stress).

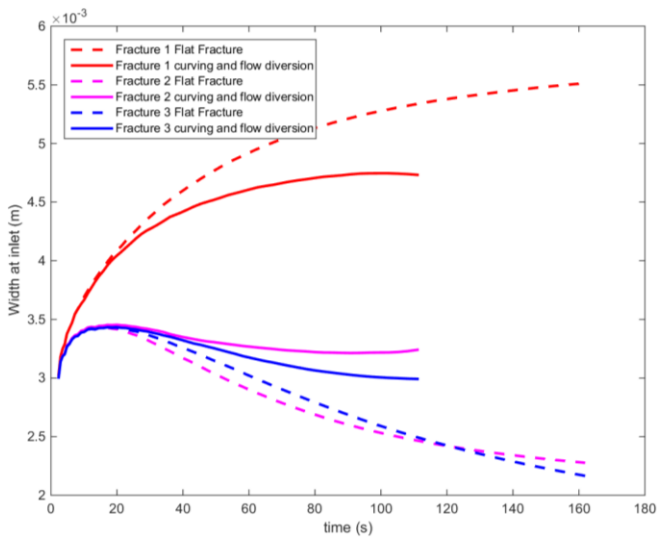


Figure 17: Fracture width at the inlet for curved fractures and the flat fractures (isotropic confining stress).

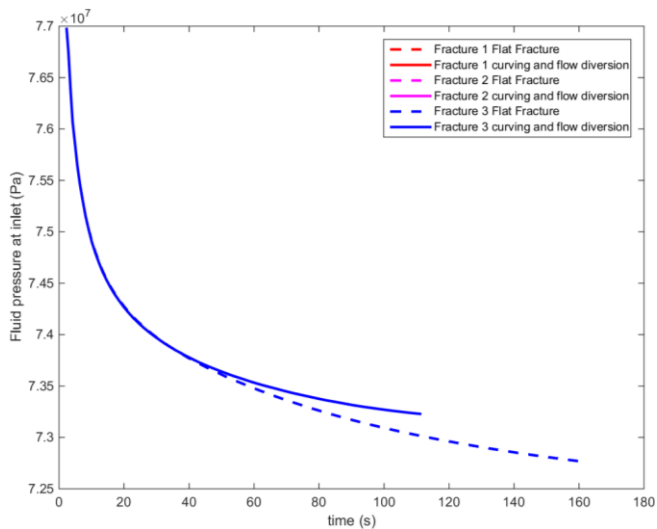


Figure 18: Fluid pressure at the inlet for curved fractures and the flat fractures (isotropic confining stress).

#### 4. CONCLUSIONS

We have described an axisymmetric XFEM algorithm with fully coupled fluid flow and elastic deformation with an implicit level set scheme to locate the fracture free boundary to satisfy the so-called  $M$ -vertex tip asymptote for propagation in the viscosity-dominated regime. The algorithm is able to model curving 3D cracks by advancing the fracture in a direction given by the maximum tensile stress at the fracture tip. By means of a specialized iterative procedure, the algorithm is able to autonomously partition the flux of fluid among the fractures in a given stage under the constraint that the fluid pressure is the same at the intersection of each of the fractures and the wellbore.

The XFEM model produced results that showed close agreement to those of a 3D DD model ILSA (Bunger and Peirce, 2014; Peirce and Bunger, 2015) that is able to model multiple planar HF that are assumed to be propagating in parallel planes with flow diversion. The capacity of the XFEM model to capture fracture curving due to mutual interaction and flux diversion was compared to an axisymmetric DD model OriBiC. The two models produced results that were in close agreement. Finally, the XFEM model was used to compare the solutions for five propagating HF in which the fractures were allowed to curve with those in which the fractures were constrained to remain parallel. In the first case, the field variables such as the fracture length, inlet fracture width, inlet flux, and wellbore pressure showed little difference between the planar fractures and those that were allowed to curve while in the second case, with isotropic confining stresses, the field variables were affected more significantly due to the fracture curving. This calls for a detailed study into various parameters involved in fracture curving and how those parameters affect the field variables. This will be the topic of a future paper where the present XFEM model will be used to explore in detail the possible conditions under which fracture curving becomes important.

#### REFERENCES

Abbas, S., E. Gordeliy, A. Peirce, B. Lecampion, D. Chuprakov, and R. Prioul. 2014. Limited height growth and reduced opening of hydraulic fractures due to fracture offsets: An XFEM Application. *SPE Hydraulic Fracturing Technology Conference*, The Woodlands, Texas, USA, SPE 168622.

Bunger, A. P. 2005. Near-surface hydraulic fracture. *Ph.D. Thesis, University of Minnesota*.

Bunger, A., E. Gordeliy, and E. Detournay. 2013. Comparison between laboratory experiments and coupled simulations of saucer-shaped hydraulic fractures in homogeneous brittle

elastic solids. *Journal of the Mechanics and Physics of Solids*, 61: 1636–1654.

Bunger, A. and A. Peirce. 2014. Numerical Simulation of Simultaneous Growth of Multiple Interacting Hydraulic Fractures from Horizontal Wells. *Shale Energy Engineering 2014*: 201-210.

Desroches, J., B. Lenoach, P. Papanastasiou, J.R.A. Pearson, M. Thiercelin, and A. Cheng. 1994. The crack tip region in hydraulic fracturing. *Proc. R. Soc. London, Ser. A*, 447: 39–48.

Detournay, E. and A. Peirce. 2014. On the moving boundary conditions for a hydraulic fracture. *International Journal of Engineering Science*, 84: 147–155.

Erdogan, F. and G. Sih. 1963. On the crack extension in plates under plate loading and transverse shear. *J. Basic Eng.*, 85: 519–527.

Fries, T.-P. and M. Baydoun. 2012. Crack propagation with the extended finite element method and a hybrid explicit–implicit crack description. *Internat. J. Numer. Methods Engrg.*, 89(12), 1527–1558.

Fries, T.-P. and T. Belytschko. 2010. The extended/generalized finite element method: an overview of the method and its applications. *Internat. J. Numer. Methods Engrg.*, 85: 253–304.

Gordeliy, E. and E. Detournay. 2011. Displacement discontinuity method for modeling axisymmetric cracks in an elastic half-space. *Int. J. Solids Struct.*, 48(19): 2614–2629.

Gordeliy, E. and A. Peirce. 2013. Implicit level set schemes for modeling hydraulic fractures using the XFEM. *Comput. Methods Appl. Mech. Engrg.*, 266: 125–143.

Gordeliy, E. and A. Peirce. 2015. Enrichment strategies and convergence properties of the XFEM for hydraulic fracture problems. *Comput. Methods Appl. Mech. Engrg.*, 283: 474–502.

Kresse, O., X. Weng, H. Gu, and R. Wu. 2013. Numerical modeling of hydraulic fracture interaction in complex naturally fractured formations. *Rock Mech. Rock Eng.*, 46(3): 555–558.

Lecampion, B. and J. Desroches. 2015. Simultaneous initiation and growth of multiple radial hydraulic fractures from a horizontal wellbore. *Journal of the Mechanics and Physics of Solids*, 82: 235–258.

Peirce, A. and A. Bunger. 2015. Interference fracturing: Non uniform distributions of perforation clusters that promote simultaneous growth of multiple hydraulic fractures, *SPE Journal*, 20: 384–395, SPE-172500.

Peirce, A. and E. Detournay. 2008. An implicit level set method for modeling hydraulically driven fractures. *Comput.*

*Methods Appl. Mech. Engrg.*, 197: 2858–2885.

Savitski, A. and E. Detournay. 1999. Propagation of a penny shape hydraulic fracture in an impermeable rock. *The 37th U.S. Symposium on Rock Mechanics (USRMS)*, Vail, Colorado, USA, ARMA-99-0851.